Pramana – J. Phys. (2021) 95:88
https://doi.org/10.1007/s12043-021-02115-y

Modelling of semiconductor laser with double external cavities for use in ultrahigh speed photonics

MOUSTAFA AHMED* and AHMED BAKRY

Department of Physics, Faculty of Science, King Abdulaziz University, 80203, Jeddah 21589, Saudi Arabia
*Corresponding author. E-mail: mostafa.farghal@mu.edu.eg

MS received 2 December 2020; revised 19 January 2021; accepted 21 January 2021

Abstract. We model and investigate the dynamics and modulation performance of semiconductor laser integrated with two short external cavities facing the front and back facets with the aim to enhance the modulation bandwidth of the laser for use in high-speed photonics. The coupled cavities provide double optical feedback (DOFB) to the laser cavity through the partially reflecting facets of the laser cavity. The study is based on modifying the rate equations of the laser to include multiple reflections of laser radiations in the external cavities. Therefore, it accounts for the regime of strong OFB that causes bandwidth enhancement. We introduce correspondence between the laser stability under DOFB and the modulation response characteristics. Also, we allocate the ranges of the DOFB that induce photon–photon resonance (PPR) effect as the main contributor to the bandwidth enhancement. We show that the intensity modulation (IM) response can be tailored by varying the reflectivity of the external mirrors when the external cavities are too short to stabilise the laser output. Modulation bandwidth better than 55 GHz is predicted under strong double OFB when the external cavities are as short as 2 mm. Stronger DOFB is found to enhance the PPR effect and induce resonant modulation over a narrow frequency range around frequencies reaching 45 GHz.

Keywords. Optical feedback; semiconductor laser; double cavity; modulation.

PACS Nos **74.40.De; 05.40.Ca; 42.55.–f**

1. Introduction

High-speed semiconductor lasers are crucially required for modern communication systems that transmit dense information with high speeds. Examples include wireless local area networks (WLANs) within radio-over fibre (RoF) systems, 100 Gbit/s Ethernet systems and interconnects in super computers and data centres [1–4]. These high-speed photonic applications require semiconductor lasers with modulation bandwidth in the millimetre-waveband which enables direct modulation of the laser with speed of several tens Gbit/s [5].

A typical constraint of increasing the modulation speed of the semiconductor laser is the carrier-photon resonance (CPR) frequency and thermal parasitics, which limit the laser bandwidth to ~20 GHz [6]. Inventive designs, such as injection locking [7,8] and modulator integration [9–11] have shown the possibility of remarkable increase in the modulation bandwidth. The authors have contributed to studies on the function of external optical feedback (OFB) to enhance the modulation bandwidth of lasers emitting from both the longitudinal edge and vertical cavity surface emitting lasers (VCSELs) [12–16]. In the regime of strong OFB, a photon–photon resonance (PPR) effect is induced between the modulating signal and a beating component of the OFB-induced resonance modes [11], which works to boost the bandwidth frequency and/or induce resonant modulation over a narrow high-frequency band [11,16–18].

Recently, the authors have contributed to bandwidth enhancement of the semiconductor laser when coupled to a very short passive cavity, predicting an increase of about 200% [16]. The extreme of short external cavity (whose resonance frequency is higher than the intrinsic relaxation frequency of the laser) is helpful to stabilise the laser dynamics [19–21] and to enable PPR under strong OFB [8]. The study was based on modifying the theory of semiconductor laser subject to OFB in which OFB was treated as time delay of laser radiation due to multiple round trips in the feedback cavity. It has been established that the PPR effect becomes stronger with strong OFB, which would contribute to further enhancement of the modulation bandwidth [12,13,16].

Published online: 19 May 2021

Therefore, the aim of this paper is to modify the coupling scheme to the semiconductor laser in such a way to strengthen OFB. We propose to couple the laser with two external short cavities in the longitudinal direction facing the front and back facets of the laser cavity. The induced double optical feedback (DOFB) then illuminates the primary laser cavity with stronger external feedback while maintaining stable operation.

We extend our previous modelling on modulation of semiconductor laser under strong OFB from single external cavity to include two external cavities. We modify the rate equations of the semiconductor laser to include light feedback coming from both cavities and explore the boundary conditions at the front and back facets and their influence on the threshold gain and phase conditions of the laser. We carry out intensive numerical integration of the developed rate equations to specify the regimes of stable dynamics of the laser over which the modulation bandwidth is enhanced. Also, we investigate the DOFB parameters that induce resonant modulation and the associated central PPR frequencies. We show that the laser operates mostly under either continuous wave (CW) or period-1 pulsation in the limit of short coupled cavities. In the former regime, strong DOFB results in PPR that works to increase the modulation bandwidth from 40 GHz of the single OFB to higher than >55 GHz using external cavities as short as 2 mm. Higher values of modulation bandwidth are predicted when the external cavity facing the front facet is equal to or shorter than the cavity facing the back facet. DOFB happens also to induce resonant modulation over a narrow frequency band centred around ∼45 GHz.

In the following section, we present the model of laser dynamics under DOFB. In §3, we introduce the procedures of numerical calculations. In §4, we present the obtained results on stability, bifurcation diagram and modulation response with bandwidth enhancement. Finally, the conclusions appear in §5.

2. Time-delay model of semiconductor laser under DOFB

The present model of semiconductor laser coupled with two longitudinal cavities is schematically illustrated in figure 1. The laser has a resonance cavity of length L_D and refractive index n_D, and is assumed to oscillate in single longitudinal mode. The laser cavity is surrounded in the longitudinal direction by two cavities. One cavity (#1) is of length L_{ex1} and is formed between the front facet of power reflectivity R_f and external reflector #1 of reflectivity R_{ex1}, while cavity #2 is of length L_{ex2} and is formed between the back facet of power reflectivity R_b and external reflector #2 of reflectivity R_{ex2}. The laser is then subjected to DOFB from the forth and back directions. Light emitted from the front facet is assumed to travel multiple round trips in the external cavity #1 and then reflected back to the laser diode with coupling efficiency η_1, and so does the light emitted from the back facet which is injected back to the laser with coupling efficiency η_2. The round trip times in the front and back external cavities are given by $\tau_1 = 2n_{\mathrm{ex1}}L_{\mathrm{ex1}}/c$ and $\tau_2 = 2n_{\mathrm{ex2}}L_{\mathrm{ex2}}/c$, respectively.

The electric components of the electric field in the laser cavity along the z-direction are assumed as

$$E(z,t) = \left[E^{(+)}(z,t) + E^{(-)}(z,t)\right]\mathrm{e}^{-j\omega t} + \text{c.c.} \quad \text{for } 0 \le z \le L_D, \tag{1}$$

where $E^{(+)}$ and $E^{(-)}$ are the forward and backward travelling components of the field with angular frequency ω. The c.c. refers to the complex conjugate quantity. In the present time-delay model, DOFB is counted as time delay of the laser light at the front facet due to the round trips in external cavity #1 and laser light at the back facet due to the round trips in external cavity #2. Therefore, the boundary conditions at the back and front facets are

$$E^{(+)}(0,t) = r_b U_2 E^{(-)}(0,t), \tag{2}$$

$$E^{(-)}(L_D,t) = r_f U_1 E^{(+)}(L_D,t), \tag{3}$$

where U_1 and U_2 are functions describing OFB induced by the front and back external cavities, respectively, and are given as

$$\begin{aligned} U_1(t-\tau_1) &= 1 - \frac{1-R_f}{R_f}\sum_{m=1}^{M}\sqrt{\eta_1 R_{\mathrm{ex1}} R_f}^{m} \\ &\quad \times \frac{E^{(+)}(L_D, t-m\tau_1)}{E^{(+)}(L_D,t)}\mathrm{e}^{-jm\psi_1} \\ &= |U_1|\,\mathrm{e}^{-j\phi_1} \end{aligned} \tag{4}$$

$$\begin{aligned} U_2(t-\tau_2) &= 1 - \frac{1-R_b}{R_b}\sum_{m=1}^{M}\sqrt{\eta_2 R_{\mathrm{ex2}} R_b}^{m} \\ &\quad \times \frac{E^{(-)}(0, t-m\tau_2)}{E^{(-)}(0,t)}\mathrm{e}^{-jm\psi_2} \\ &= |U_2|\,\mathrm{e}^{-j\phi_2}, \end{aligned} \tag{5}$$

where the summation is taken over the number of round trips from $m = 1$ to M. The phases ϕ_1 and ϕ_2 are the phases of the complex OFB functions U_1 and U_2, respectively. The phases ψ_1 and ψ_2 of the feedback function are given by

$$\psi_1 = \phi_f + \phi_{\mathrm{ex1}} + \omega\tau_1 \tag{6}$$

$$\psi_2 = \phi_b + \phi_{\mathrm{ex2}} + \omega\tau_2. \tag{7}$$

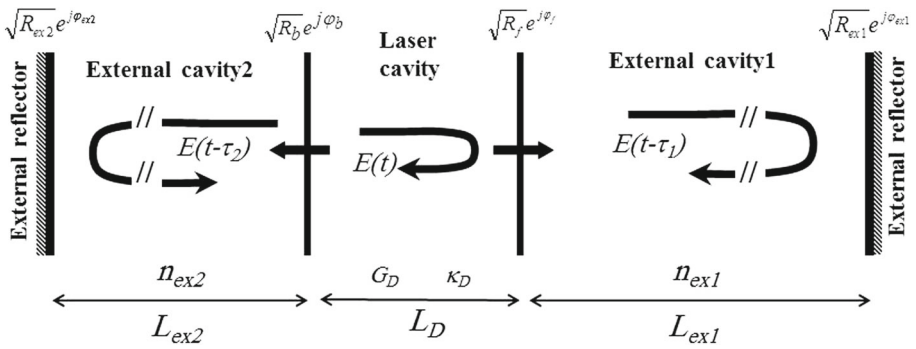

Figure 1. Scheme of a semiconductor laser sandwiched between two sequent external cavities. $E(t)$ is the electric field at instant t, $E(t-\tau_1)$ is the delayed electric field at instant t after delay time τ_1 in cavity #1, $E(t-\tau_2)$ is the delayed electric field at instant t after delay time τ_2 in cavity #2, L_D, n_D are the length and refractive index of laser cavity, g_D, κ_D, β_D are the gain per unit length, internal loss and propagation constant of laser cavity, L_{ex1}, L_{ex2} are the length of feedback cavity #1 and cavity #2, n_{ex1}, n_{ex2} are the refractive index of feedback cavity #1 and cavity #2, R_f, R_b are the power reflectivity at the front and the back facets and R_{ex1}, R_{ex2} are the power reflectivity at reflector #1 and reflector #2.

The last terms $\omega\tau_1$ and $\omega\tau_2$ correspond to the time-delay phase changes due to the round trips of laser radiation in external cavities #1 and 2, respectively.

By substituting the definitions of the forward $E^{(+)}$ and backward $E^{(-)}$ components of the field in the laser cavity

$$E^{(+)}(z,t) = E^{(+)}(0,t) \times \exp\{(g_D-\kappa_D)z/2 - j\beta_D z\} \quad (8)$$

$$E^{(-)}(z,t) = E^{(-)}(L_D,t) \times \exp\{(g_D-\kappa_D)(L_D-z)/2 - j\beta_D(L_D-z)\} \quad (9)$$

and the oscillation condition of the lasers under the DRFB becomes

$$1 = \sqrt{R_f R_b}\,|U_1|\,|U_2| \times \exp\{(g_D-\kappa_D)L_D\} \times \exp\left\{-j\left(2\beta_D L_D + \varphi_f + \varphi_b + \phi_1 + \phi_2\right)\right\} \quad (10)$$

which is then separated into the following gain and phase conditions at the threshold:

$$G_{th} = G_{thD} - \frac{c}{n_D L_D} \times \left[\ln|U_1(t-\tau_1)| + \ln|U_2(t-\tau_2)|\right], \quad (11)$$

$$2\beta_D L_D + \varphi_f + \varphi_b + \phi_1 + \phi_2 = 2q\pi, \quad (12)$$

where q is an integer. In eq. (11), $G_{thD} = (c/n_D)\,g_{thD}$ is the threshold gain per second in the solitary (without OFB) laser and g_{thD} is the corresponding gain per unit length, which is determined by the total loss in the cavity as

$$g_{thD} = \kappa_D + \frac{1}{2L_D}\ln\frac{1}{R_f R_b}. \quad (13)$$

Equation (11) then denotes variation of the laser threshold G_{th} due to DOFB, which is responsible for the complexity in the laser dynamics.

By denoting the electric field $E(z,t)$ in the laser cavity as a time-harmonic field with a slowly time-varying amplitude $\widehat{E}(t)$ as

$$E(r,t) = \widehat{E}(t)\,\Phi(r)\,\mathrm{e}^{j\omega t} + \text{c.c.} \quad (14)$$

with $\Phi(r)$ being the spatial field distribution of the field in the laser cavity and substituting it in Maxwell's equations, we obtain the following rate equation of $E(t)$ [22]:

$$\frac{\mathrm{d}\widehat{E}}{\mathrm{d}t} = \frac{1}{2}(1+j\alpha)(\Gamma G - G_{th})\widehat{E}, \quad (15)$$

where G is the optical gain per second and a is its slope versus variation in the injected carrier number N. Γ is the confinement factor of the field in the active region whose volume is V, N_{th} is the carrier number at the threshold and α is the linewidth enhancement factor. The second term describes the phase variation by the stimulated emission, which represents the imaginary part of susceptibility [22]. $G_{th} = (c/n_D)\,g_{th}$ is the threshold gain per unit length, and is then determined by the feedback functions U_1 and U_2 as given in threshold-gain condition (11). In this approach and at time t, the amplitudes of the time-delayed propagating fields $E^{(+)}(L_D, t-m\tau_1)$ and $E^{(-)}(0, t-m\tau_2)$ in eqs (4) and (5) are replaced by the slowly time-varying amplitudes $\widehat{E}(t-m\tau_1)$ and $\widehat{E}(t-m\tau_2)$, respectively, and the amplitudes $E^{(+)}(L,t)$ and $E^{(-)}(0,t)$ change to $\widehat{E}(t_1)$. Therefore, the double OFB U_1 and U_2 in eqs (4) and (5) are rewritten as

$$U_1(t-\tau_1) = |U_1|\,\mathrm{e}^{-j\phi_1} = 1 - \frac{1-R_f}{R_f}\sum_{m=1}^{M}\sqrt{\eta_1 R_{\mathrm{ex1}} R_f}^{m} \times \frac{\widehat{E}(t-m\tau_1)}{\widehat{E}(t)}\mathrm{e}^{-jm\psi_1} \tag{16}$$

$$U_2(t-\tau_2) = |U_2|\,\mathrm{e}^{-j\phi_2} = 1 - \frac{1-R_b}{R_b} \times \sum_{m=1}^{M}\sqrt{\eta_2 R_{\mathrm{ex2}} R_b}^{m}\frac{\widehat{E}(t-m\tau_2)}{\widehat{E}(t)}\mathrm{e}^{-jm\psi_2}. \tag{17}$$

Rate equation (15) can be transformed to a couple of equations for the photon number $S(t)$ contained in the lasing mode and the phase $\theta(t)$ by writing the complex field amplitude with the phase term as

$$\widehat{E}(t) = \left|\widehat{E}(t)\right|\mathrm{e}^{j\theta(t)} \tag{18}$$

with $S(t) \propto \left|\widehat{E}(t)\right|^2$. Therefore, the following rate equations are obtained:

$$\frac{\mathrm{d}S}{\mathrm{d}t} = \frac{1}{2}\left[\Gamma G - G_{thD} + \frac{c}{n_D L_D}\left[\ln|U_1(t-\tau_1)| + \ln|U_2(t-\tau_2)|\right]\right]S + \Gamma R_{\mathrm{SP}} \tag{19}$$

$$\frac{\mathrm{d}\theta}{\mathrm{d}t} = (\omega_\ell - \omega) + \frac{\alpha}{2}(\Gamma G - G_{thD}) - \frac{c}{2n_D L_D}(\phi_1+\phi_2) = (\omega_\ell-\omega) + \frac{\alpha}{2}(\Gamma G - G_{thD}) - \frac{c}{2n_D L_D}\left[\arg(U_1) + \arg(U_2)\right] \tag{20}$$

which in addition to the following rate equation of N describe the laser dynamics.

$$\frac{\mathrm{d}N}{\mathrm{d}t} = \frac{I}{e} - \frac{N}{\tau_s} - GS. \tag{21}$$

The optical gain G is defined by including the gain suppression as

$$G = \frac{a}{V}\frac{N-N_g}{1+\varepsilon S}, \tag{22}$$

where ε is the gain suppression factor. In the above rate equations, R_{SP} is the rate of inclusion of the spontaneous emission into the lasing mode, I is the injection current, τ_s is the electron lifetime due to spontaneous emission and e is the electron charge. In eq. (20), the first term represents the frequency chirp due to the variation of the lasing angular frequency ω in the presence of OFB from the free angular oscillation frequency ω_ℓ [23], while the last term represents the chirp originating from the feedback functions U_1 and U_2. The forms of these functions U_1 and U_2 suitable for rate equations (16) and (17) are rewritten as

$$U_1(t-\tau_1) = |U_1|\,\mathrm{e}^{-j\phi_1} = 1 - \frac{1-R_f}{R_f}\sum_{m=1}^{M}\sqrt{\eta_1 R_{\mathrm{ex1}} R_f}^{m} \times \sqrt{\frac{S(t-m\tau_1)}{S(t)}}\frac{\mathrm{e}^{j\theta(t-m\tau_1)}}{\mathrm{e}^{j\theta(t)}}\mathrm{e}^{-jm\psi_1} \tag{23}$$

$$U_2(t-\tau_2) = |U_2|\,\mathrm{e}^{-j\phi_2} = 1 - \frac{1-R_b}{R_b}\sum_{m=1}^{M}\sqrt{\eta_2 R_{ex2} R_b}^{m} \times \sqrt{\frac{S(t-m\tau_2)}{S(t)}}\frac{\mathrm{e}^{j\theta(t-m\tau_2)}}{\mathrm{e}^{j\theta(t)}}\mathrm{e}^{-jm\psi_2}. \tag{24}$$

In this case, the terms $\exp\{j[\theta(t-m\tau_1)-\theta(t)]\}$ and $\exp\{j[\theta(t-m\tau_2)-\theta(t)]\}$ represent deviations in the optical phase due to chirping induced by time delay in the external cavities #1 and 2, respectively. The present model takes into account multiple reflections through both external cavities which add to the complexity of the model. Therefore, the present modelling can analyse cases of strong DOFB, for example semiconductor lasers with antireflecting coated facets used as the pumping sources in fibre-grating lasers [24], and lasers used in radio-over fibre links to enhance the modulation bandwidth and/or induce high-frequency resonance modulation [12].

3. Numerical calculations

The laser dynamics under the longitudinal DOFB are simulated by numerical integration of rate equations (19)–(21) by means of the fourth-order Runge–Kutta method. The time step of integration is set to be 0.5 ps and the integration is carried out over a period of $T = 3{-}5\,\mu$s over which the operation reaches steady state. The calculations are done for 1.55-μm InGaAsP laser coupled with two air feedback cavities on both longitudinal sides. Numerical values of the laser parameters are listed in table 1. The corresponding threshold current is $I_{th0} = 10.5$ mA. These parameters were found to correspond to modulation bandwidth of the solitary laser (without OFB) as high as 27 GHz when the bias current is 49 mA [25]. Two external air cavities are assumed with lengths as short as $L_{\mathrm{ex1}} = 2$ mm and $L_{\mathrm{ex2}} = 3$ mm, which correspond to time delays $\tau_1 = 13.3$ ps and $\tau_2 = 20$ ps and external cavity resonance frequency spacing of $1/\tau_1 = 75$ GHz and $1/\tau_1 = 50$ GHz, respectively.

Table 1. Values of the parameters of 1.55 μm InGaAsP lasers used in calculations.

Parameter	Value	Unit
Tangential coefficient of gain, a	8.25×10^{-12}	m^3s^{-1}
Electron number at transparency, N_g	5.12×10^7	–
Gain suppression factor, ε	9.2×10^{-7}	–
Electron lifetime, τ_s	796	ps
Threshold gain in primary laser cavity G_{thD}	5.92×10^{11}	s^{-1}
Rate of spontaneous emission R_{SP}	2.0×10^{12}	s^{-1}
Linewidth enhancement factor, α	3.5	–
Refractive index of the active region, n_D	3.513	–
Length of the active region, L_D	120	μm
Volume of the active region, V	30	μm^3
Field confinement factor, Γ	0.15	–
Reflectivity at the front facet, R_f	0.2	–
Reflectivity at the back facet, R_b	0.6	–

4. Results and discussions

4.1 *Steady-state solutions of laser rate equations*

The steady-state solutions of eqs (19) and (20) are

$$G - G_{thD} = -\frac{c}{n_D L_D}\ln\left(|U_1||U_2|\right) - \frac{\Gamma R_{SP}}{S} \approx -\frac{c}{n_D L_D}\ln\left(|U_1||U_2|\right), \quad (25)$$

$$0 = (\omega_\ell - \omega) + \frac{\alpha}{2}(G - G_{thD}) - \frac{c}{2n_D L_D}\left[\arg(U_1) + \arg(U_2)\right], \quad (26)$$

where the rate of spontaneous emission R_{SP} is ignored in eq. (25) compared to that of the stimulated emission to simplify the calculation. The phase variations under DOFB are then determined as the solution of the following equation:

$$\omega_\ell \tau - \omega\tau = \frac{c\tau}{2n_D L_D} \times \left[\alpha\ln(|U_1||U_2|) + \arg(U_1 + U_2)\right] = \frac{\tau}{\tau_{in}}\left[\alpha\ln(|U_1||U_2|) + \arg(U_1 + U_2)\right], \quad (27)$$

where $\tau_{in} = 2n_D L_D/c$ is the round trip time in the laser cavity. The above equation may have multiple solutions depending on the strength of OFB, which correspond to oscillation of the laser in multiple external modes. The appropriate solution will be the one that corresponds to lower level of the threshold gain G_{th}. The steady-state values of the carrier number $\overline{N}$ and photon number $\overline{S}$ are obtained by solving the steady-state version of rate equations (19) and (21) of $S(t)$ and $N(t)$, respectively, as

$$\overline{N} = N_g + \frac{1+\varepsilon\overline{S}}{\frac{\Gamma a}{V}}\left[G_{thD} - \frac{c}{n_D L_D}\ln\left(|U_1||U_2|\right)\right]. \quad (28)$$

$$\overline{S} = \frac{1}{1+\frac{\varepsilon}{\frac{\Gamma a}{V}\tau_e}}\left[\frac{\frac{I}{e} - \frac{N_0}{\tau_s}}{G_{thD} - \frac{c}{n_D L_D}\ln(|U_1||U_2|)} - \frac{1}{\frac{\Gamma a}{V}\tau_s}\right]. \quad (29)$$

The feedback functions U_1 and U_2 are calculated using the solutions of phases $\omega\tau_1$ and $\omega\tau_2$ as given in eqs (6), (7), (16) and (17).

Examples of the steady-state calculations as functions of the reflectivity $\eta_2 R_{ex2}$ of external mirror #2 is given in figure 2 using reflectivity of external mirror #1 of $\eta_1 R_{ex1} = 0.04$. This level of OFB corresponds to CW operation of the laser when it is subjected to feedback from external mirror #1 only. Figures 2a–2c correspond to three cases of $L_{ex2} = 3$ mm ($> L_{ex1}$), $L_{ex1} = L_{ex2} = 2$ mm and $L_{ex2} = 0.5$ mm ($< L_{ex1}$), respectively, which help to clarify the influence of the time delay on the steady-state characteristics. The figures plot variations of the photon number $\overline{S}$ and frequency chirp $\Delta\omega = \omega_\ell - \omega$ with variation of ηR_{ex2}. Each of these solutions corresponds to the minimum level of threshold gain at the corresponding value of $\eta_2 R_{ex2}$. Figure 2a indicates that both $\overline{S}$ and $\Delta\omega$ are almost constant in the regime of low reflectivity ηR_{ex2}, indicating stable dynamics of the laser. Then both $\overline{S}$ and $\Delta\omega$ jump to higher values over the range $\eta_2 R_{ex2} = 0.265$–0.57, which indicates that OFB becomes strong enough to excite resonance modes in the external cavity and the laser is expected to jump to one of these modes. If $\eta_2 R_{ex2}$ increases further, both $\overline{S}$ and $\Delta\omega$ decrease with the increase of $\eta_2 R_{ex2}$. However, they still maintain values larger than those of the regime of weak reflectivity $\eta_2 R_{ex2}$. This rise and drop of both $\overline{S}$ and $\Delta\omega$ indicate

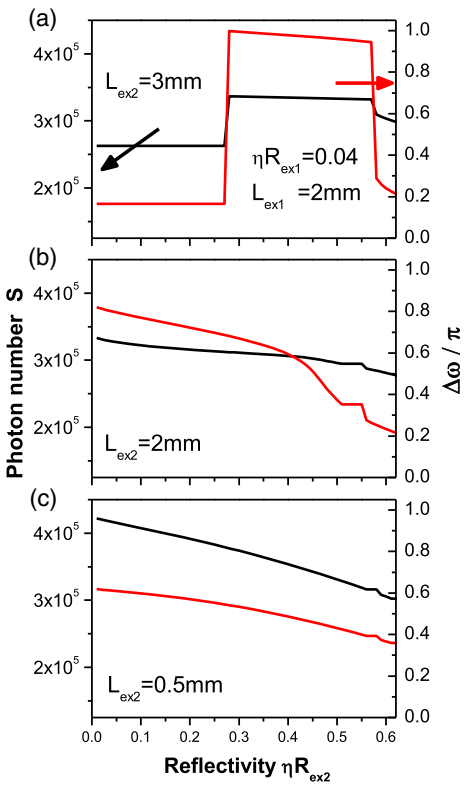

Figure 2. Steady-state solutions of the non-modulated laser under DOFB: photon number $\overline{S}$ and frequency chirp $\Delta\omega$ as functions of reflectivity $\eta_2 R_{ex2}$ with $\eta_1 R_{ex1} = 0.04$ and $L_{ex1} = 2$ mm when (**a**) $L_{ex2} = 3$ mm, (**b**) $L_{ex2} = 2$ mm and (**c**) $L_{ex2} = 0.5$ mm.

that the laser is attracted to a route to instability [26]. These conclusions will be confirmed in the next subsection, which shows that the laser is attracted to a route to chaos. OFB happens to induce internal and external modes and the relaxation oscillation modes in addition to their sums and differences [27–29] and the laser may jump to one or more of these modes depending on the OFB parameters. DOFB parameters include strength of OFB from either external cavity, length of the two cavities and phases of injected light compared with the phase of light inside the laser cavity. Chaotic laser oscillates at the mixed frequencies of the internal and external modes and the relaxation oscillation mode [26].

In figure 2b where $L_{ex1} = L_{ex2} = 2$ mm, $\overline{S}$ decreases slowly with the change of $\eta_2 R_{ex2}$, and so does the frequency chirp $\Delta\omega$ but after $\eta_2 R_{ex2} = 0.35$. $\Delta\omega$ drops to lower values with the increase of $\eta_2 R_{ex2}$. These results could be an indicator of instabilities of the laser dynamics under strong OFB of $\eta_2 R_{ex2} = 0.35$, but such instabilities are not so sever as in the case of $L_{ex2} = 3$ mm ($> L_{ex1}$) in figure 2b. In figure 2c where $L_{ex2} = 0.5$ mm ($< L_{ex1}$), both $\overline{S}$ and $\Delta\omega$ decrease slowly with the change of $\eta_2 R_{ex2}$ over the relevant range of $\eta_2 R_{ex2}$ which could indicate that the addition of OFB from mirror #2 may not change the CW operation of the laser under OFB from mirror #1.

4.2 *Dynamics and stability of the non-modulated laser*

In this subsection, we study the oscillation behaviour of the non-modulated laser when subjected to the double OFB. The study is given in terms of the bifurcation diagram of the emitted photon number $S(t)$. Figures 3a–3d plot the bifurcation diagrams of the non-modulated laser in terms of the power reflectivity $\eta_2 R_{ex2}$ of external reflector #2 when $\eta_1 R_{ex1} = 0.04, 0.06, 0.08$ and 0.1, respectively. When the laser is coupled to cavity #2 with these levels of OFB, it is characterised by CW operation. The bifurcation diagram is constructed by picking up the peak S_{peak} of the photon number $S(t)$, normalised by its average value $\overline{S}$, when the feedback induces time variation of $S(t)$ and plotting $S_{peak}/\overline{S}$ vs. $\eta_2 R_{ex2}$. As shown in figure 3a, the laser operates under CW in the regime of weak OFB (low values of $\eta_2 R_{ex2}$). The feedback strength of $\eta_2 R_{ex2} = 0.265$ behaves like a Hopf-bifurcation point at which the laser starts to emit period-1 pulsation which extends over the period of $\eta_2 R_{ex2} = 0.265$–0.57. Since the laser operates in CW under OFB of $\eta_2 R_{ex1} = 0.04$ from external mirror #1, the induced pulsation corresponds to external cavity #2. When $\eta_2 R_{ex2}$ reaches 0.58, the bifurcation diagram indicates a chaotic state. That is, the laser is attracted to a route-to-chaos under strong OFB [30,31]. These results are in good agreement with the steady-state stability results and discussion of figure 2a. Examples of the temporal trajectories of the laser intensity in the investigated dynamic states of CW, period-1 oscillation and chaos are shown in figures 4a–4c, respectively. In figure 4a, the CW operation is characterised by a constant value of the photon number $S(t)$. In this case, the laser exhibits transient damped oscillations due to CPR before it relaxes to the steady state. The frequency of these relaxation oscillations is comparable to that of the CPR of the solitary laser $f_{CP0} = 7$ GHz. In figure 4b, the laser output is a periodic self-pulsation with a frequency of $f_{SP} = 43$ GHz, which is, much higher than the CPR frequency. That is, the laser jumps to one of the external cavity modes excited by DOFB. In figure 4c, the chaotic dynamics are characterised by irregular variation of $S(t)$ with time variation. Chaos could be explained as a competition between the internal laser resonance and the resonances in the external cavities [32].

It is useful to correlate the characteristics of the bifurcation diagram of figure 3a when $\eta_2 R_{ex2} = 0.04$ with the corresponding steady-state solutions plotted in figure 2a. The regime of constant values of $\overline{S}$ and $\Delta\omega$

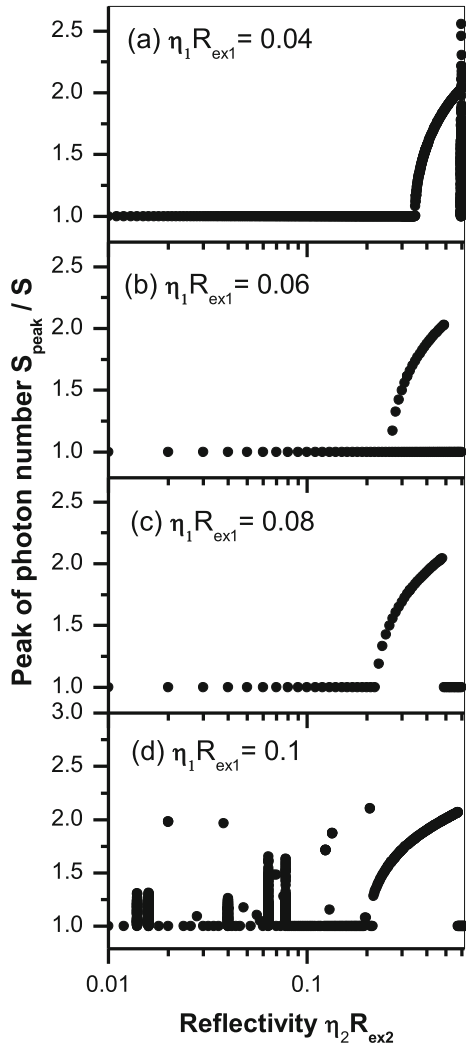

Figure 3. Bifurcation diagram of the non-modulated laser under double feedback in terms of $\eta_2 R_{ex2}$ when (**a**) $\eta_1 R_{ex1} = 0.04$, (**b**) $\eta_1 R_{ex1} = 0.06$, (**c**) $\eta_1 R_{ex1} = 0.08$ and (**d**) $\eta_1 R_{ex1} = 0.1$.

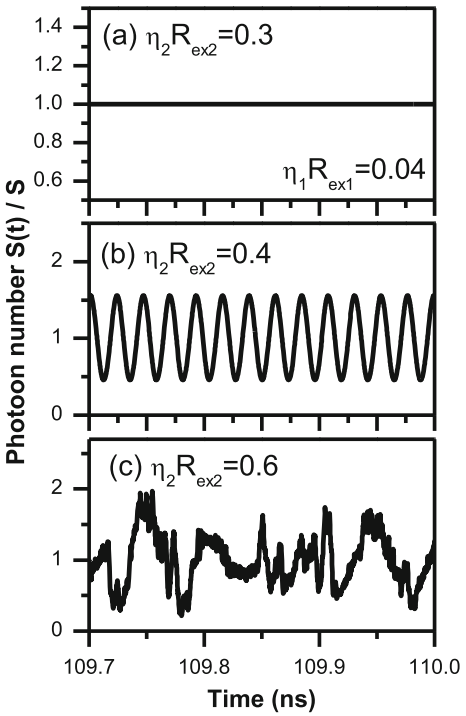

Figure 4. Temporal trajectories of the photon number $S(t)$ when (**a**) $\eta_2 R_{ex2} = 0.3$ (CW), (**b**) $\eta_2 R_{ex2} = 0.4$ (period-1 pulsation) and (**c**) $\eta_2 R_{ex2} = 0.6$ (chaos) that correspond to the bifurcation diagram of figure 3a.

in figure 2 corresponds to the stable CW operation when $\eta_2 R_{ex2} \leq 0.26$. The Hopf bifurcation point of $\eta_2 R_{ex2} = 0.265$ in figure 3a corresponds to the values of $\eta_2 R_{ex2}$ in figure 2 at which the laser jumps to one of the induced external cavity modes. This regime of laser oscillations in external cavity mode(s) corresponds to the regime of self-pulsation in figure 3a. As shown in figure 3a, this regime is terminated and the laser exhibits chaotic dynamics when $\eta_2 R_{ex2} = 0.59$ which is the same value at which the laser intensity and phase ($\overline{S}$ and $\Delta\omega$) abruptly decrease in figure 2a.

Figures 3b and 3c indicate bifurcation diagrams similar to that in figure 3a without revealing the chaos state. Instead, the laser restores the CW operation with further increase of $\eta_2 R_{ex2}$ beyond the regime of period-1 pulsation. The figures indicate that the increase in the value of $\eta_1 R_{ex1}$ to 0.06 and 0.08 results not only in shifting the Hopf bifurcation point to lower values of $\eta_2 R_{ex2}$ but also in shorting the range of $\eta_2 R_{ex2}$ over which the laser emits period-1 pulsation. In these two cases, the strong DOFB induces period-1 oscillations and the lasing mode jumps to external cavity modes without exhibiting unstable oscillations or mode hopping that characterises chaotic dynamics [26]. This pulsation corresponds to regime V in the classification of laser dynamics under OFB developed by Tkach and Chraplyvy [21]. On the other hand, figure 3d of stronger feedback from mirror #1, $\eta_1 R_{ex1} \leq 0.1$, indicates instabilities and chaos in the intermediate range of $\eta_1 R_{ex1}$. That is, strong DOFB induces instabilities in the laser dynamics, which could be associated with hopping among the variety of modes of either or both external cavities [26].

The bifurcation diagrams in figures 5a and 5b can add more clarification to the influence of time delay in the two external cavities on the laser output, which correspond to the cases of $L_{ex2} = L_{ex1} = 2$ mm and $L_{ex2} = 2$ mm ($< L_{ex1}$), respectively. The feedback from mirror #1 is kept at the same strength of figure 3 ($\eta_1 R_{ex1} = 0.04$). Figure 5a indicates that the laser operates in CW up to $\eta_2 R_{ex2} = 0.36$, and then emits period-1 pulsation up to $\eta_2 R_{ex2} = 0.6$ beyond

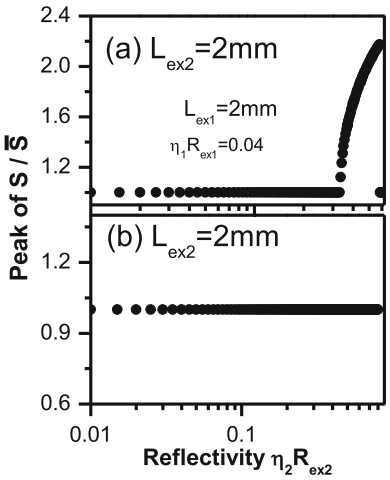

Figure 5. Bifurcation diagram of the non-modulated laser under double feedback in terms of $\eta_2 R_{ex2}$ when (**a**) $L_{ex2} = 2$ mm and (**b**) $L_{ex2} = 0.5$ mm, using $\eta_1 R_{ex1} = 0.04$ and $L_{ex1} = 2$ mm.

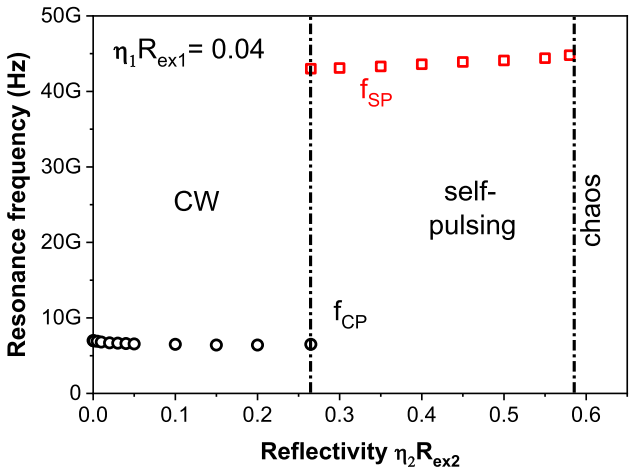

Figure 6. Resonance frequency in the laser oscillation in both the CW regime (relaxation CPR frequency) and self-pulsing oscillation as functions of reflectivity $\eta_2 R_{ex2}$ when $\eta_1 R_{ex1} = 0.04$.

which the pulsation is damped again and the CW operation is restored. In this case, the chaotic dynamics of the case of $L_{ex2} > L_{ex1}$ in figure 3a are not represented. These finding are again in good correspondence with the steady-state analysis in figure 2b. However, similar to the case of $L_{ex2} = 3$ mm $> L_{ex1}$ the increase of the feedback to $\eta_1 R_{ex1} \geq 0.9$ results in instabilities in the laser output like those presented in figure 3d. On the other hand, figure 5b of $L_{ex2} = 0.5$ mm ($<L_{ex1}$) indicates CW operation over the relevant range of feedback $\eta_2 R_{ex2}$, which supports the predicted stable operation in figure 3c. In this case, however, the increase of feedback from mirror #1 induces period-1 pulsation over a narrow range of $\eta_2 R_{ex2}$ in the regime of weaker feedback ($\eta_2 R_{ex2} < 0.1$). Instabilities in the laser operation including chaotic dynamics are induced when the feedback from mirror #1 becomes as strong as $\eta_1 R_{ex1} \geq 0.15$. In conclusion, the laser operation under DOFB is more stable when the time delay of laser radiation in the external cavity facing the back facet of the laser cavity is shorter than that in the external cavity facing the front facet, and instabilities are induced at stronger levels of DOFB.

It is worthy to gain insight into the resonance frequency of the laser oscillations over the relevant range of reflectivity $\eta_2 R_{ex2}$. This relationship is plotted in figure 6 for the bifurcation diagram of figure 3a when $\eta_1 R_{ex1} = 0.04$. The figure shows little variation of the frequency f_{CP} of the damped relaxation oscillations that characterise the CW operation as long as $\eta_2 R_{ex2} \leq 0.26$. At the bifurcation point of $\eta_2 R_{ex2} = 0.265$, the laser exhibits two oscillation components, one component is with low frequency of $f_{CP} = 6.7$ GHz that corresponds to the relaxation oscillations while the other component is with higher frequency of $f_{SP} = 43$ GHz of self-pulsation. In the regime of self-pulsation, the oscillation frequency f_{SP} increases with the increase of $\eta_2 R_{ex2}$ reaching $f_{SP} = 45.5$ GHz when $\eta_2 R_{ex2} = 0.57$. These DOFB-induced high-frequency oscillations is the main cause of the PPR effect in semiconductor laser under OFB [16] as will be discussed below.

4.3 *Modulation characteristics under DOFB*

In this subsection, we assume that the laser is subjected to the current modulation $I(t) = I_b + I_m \sin(2\pi f_m t)$ in rate equation (21), where I_b is the biasing current of the laser and I_m is the amplitude of the signal (modulation current) whose frequency is f_m. The calculated IM response corresponds to the regime of small-signal modulation for which we set $I_m = 0.01 I_b$. In figure 7a, we present examples of the IM-response spectra with higher bandwidth when the laser under DOFB is operating in the state of CW. DOFB corresponds to $\eta_1 R_{ex1} = 0.04$ and $\eta_2 R_{ex2}$ ranging between 0.02 and 0.3. The IM response of the laser with single OFB from cavity #1 is also plotted to discriminate the modulation improvement due to OFB from cavity #2. In such a case, the bandwidth is $f_{3\,dB} = 40$ GHz while the CPR peak occurs around $f_{CP} = 15$ GHz. The figure shows that whilst OFB from mirror #2 shares variation of the laser threshold, several changes are seen that characterise the IM response. The CPR peak frequency decreases with the increase of $\eta_2 R_{ex2}$; $f_{CP} = 14$ GHz when $\eta_2 R_{ex2} = 0.02$ while it decreases to $f_{CP} = 11$ GHz when $\eta_2 R_{ex2} = 0.3$. As the CPR frequency is proportional to the square root of the threshold gain [5], this

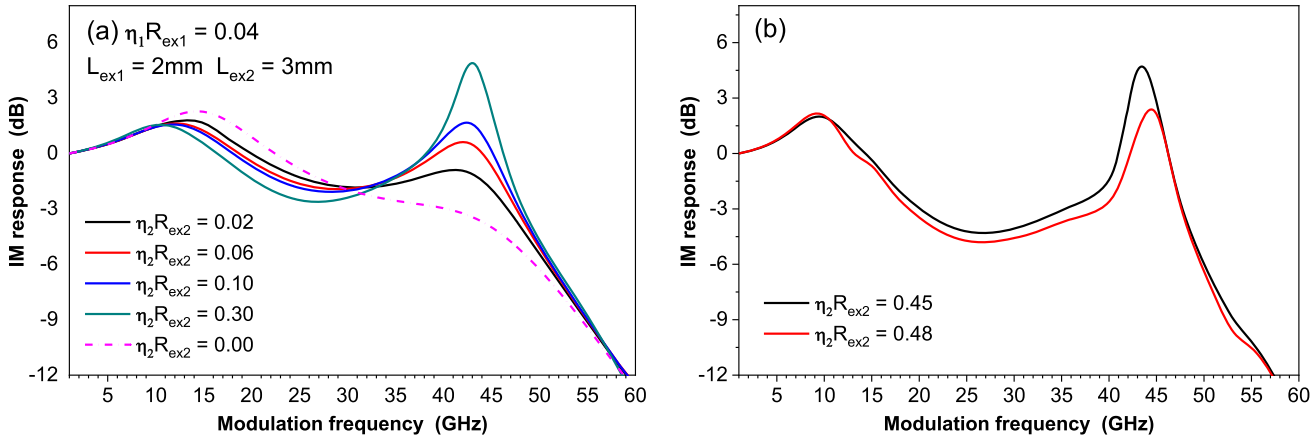

Figure 7. IM response spectra of the laser under DOFB with (**a**) bandwidth enhancement when $\eta_2 R_{ex2} = 0.02-0.3$ and (**b**) resonant modulation when $\eta_2 R_{ex2} = 0.45$ and 0.48.

reduction of the CPR frequency indicates that the amplitude and phase of OFB at the laser facet as well as their coupling work to lower the level of threshold gain. The response spectra exhibit another peak stronger than the CPR peak at much higher frequency without dropping the IM response below the –3 dB level. This peak frequency increases from 41 GHz when $\eta_2 R_{ex2} = 0.02$ to 43 GHz when $\eta_2 R_{ex2} = 0.3$. These high-frequency peaks correspond to PPR of the laser; thanks to modulation at frequencies close to the beating frequency of the resonance modes excited by the DOFB as discussed before. The coupling between these modes occurs due to the carrier pulsation introduced by the applied modulation signal at their beating frequency and introduces resonance in the IM response at this frequency [16,17]. The PPR effect becomes stronger and the response peak becomes higher with the increase in $\eta_2 R_{ex2}$. As seen in the figure, the difference in the peak height is nearly 4 dB when the reflectivity $\eta_2 R_{ex2}$ increases from 0.05 to 0.5. The increase in the PPR frequency is interestingly associated with the enhancement of the 3dB bandwidth; bandwidth is escalated to $f_{3\,dB} = 46.5$ GHz when $\eta_2 R_{ex2} = 0.02$ which is enhanced to $f_{3\,dB} = 48.5$ GHz when $\eta_2 R_{ex2} = 0.3$.

Figure 7b plots IM responses with other spectral characteristics induced when the laser is attracted to self-pulsation in the bifurcation diagram of figure 3a. In this case, the response enhancement around the PPR frequency is limited to a passband and the PPR peak is separated from the CPR peak via a gap with response $<$ –3dB. Ahmed *et al* [12] called this type of modulation response as 'resonant modulation'. The two response spectra plotted in figure 7b correspond to $\eta_2 R_{ex2} = 0.45$ and 0.48, which correspond to the shift of the PPR frequency from $f_{PP} = 43.5$ to 44.5 GHz. The figure indicates that this type of resonant modulation is associated with the narrowing of the modulation bandwidth to values around $f_{3\,dB} = 20$ GHz. The height of the PPR peak when $\eta_2 R_{ex2} = 0.48$ is lower than that of the peak when $\eta_2 R_{ex2} = 0.45$ which is due to the higher harmonic distortion of the modulated signal that increases the power of higher harmonics at the expense of the power at the fundamental frequency [33]. The values of the second and third harmonic distortions are –22.4 dB and –20.3 dB when $\eta_2 R_{ex2} = 0.45$ which increase to –22.6 dB and –26.3 dB when $\eta_2 R_{ex2} = 0.48$. The modulation is then efficient within the narrow frequency band of (35–48 GHz) when $\eta_2 R_{ex2} = 0.45$ which is limited more to (40–48 GHz) when $\eta_2 R_{ex2} = 0.48$.

Figure 8 plots variation of the modulation bandwidth $f_{3\,dB}$ with the reflectivity $\eta_2 R_{ex2}$ of external mirror #2 at two values of OFB from mirror #1 ($\eta_1 R_{ex1} = 0.04$ and 0.08). For both cases of $\eta_1 R_{ex1}$ the figure shows the increase of $f_{3\,dB}$ with the increase of $\eta_2 R_{ex2}$ in the regime of bandwidth enhancement when the laser operates in CW. The maximum predicted value of $f_{3\,dB}$ is 48.5 GHz when $\eta_1 R_{ex1} = 0.04$ and increases to 51 GHz when $\eta_1 R_{ex1} = 0.08$. In the regime of resonant modulation induced by PPR the bandwidth abruptly decreases to values smaller than 25 GHz, as discussed for figure 7b.

Now, we investigate the influence of OFB from mirror #1 on the spectral characteristics of the IM response. Figure 9 plots examples of improved IM responses when the reflectivity of external mirror #2 is fixed at $\eta_2 R_{ex2} = 0.07$ while the reflectivity $\eta_1 R_{ex1}$ increases between 0.01 and 0.09. The figure shows the case of further enhancement of the modulation bandwidth; $f_{3\,dB}$ increases between $f_{3\,dB} = 40$ GHz and 51.5 GHz with the relevant strengthening of $\eta_1 R_{ex1}$. This increase of the bandwidth is associated with the shift of the PPR peak frequency to higher frequency; $f_{PP} = 35$ GHz

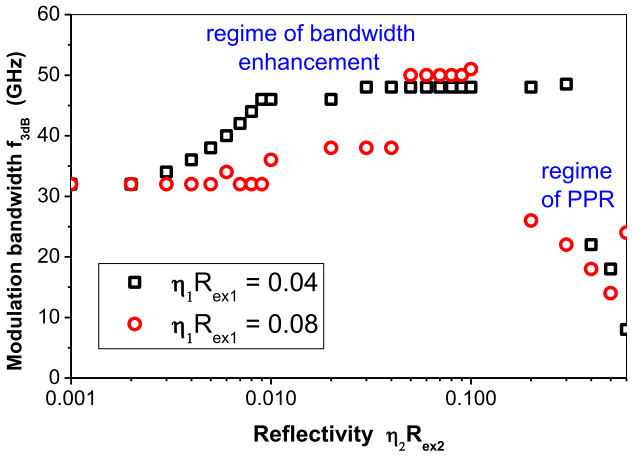

Figure 8. Variation of modulation bandwidth $f_{3\,\mathrm{dB}}$ with reflectivity $\eta_2 R_{\mathrm{ex2}}$ of external mirror #2 when $\eta_1 R_{\mathrm{ex1}} = 0.04$ and 0.08 over both regimes of bandwidth enhancement and resonant modulation.

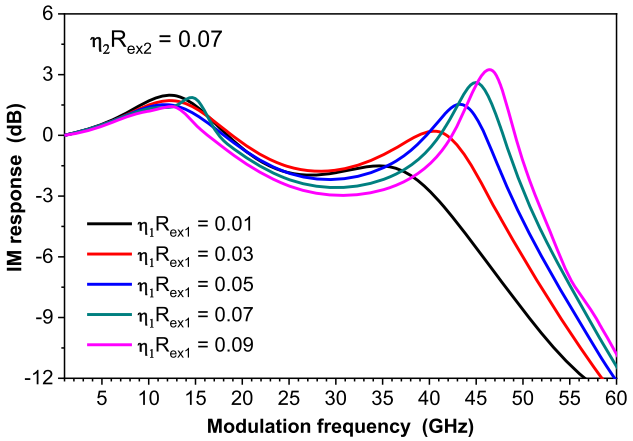

Figure 9. IM response spectra of the laser showing bandwidth enhancement under double OFB at different reflectivities of external mirror #1 of $\eta_1 R_{\mathrm{ex1}} = 0.01$–$0.0$ when $\eta_2 R_{\mathrm{ex2}} = 0.07$.

when $\eta_2 R_{\mathrm{ex2}} = 0.01$ while $f_{\mathrm{PP}} = 47$ GHz when $\eta_2 R_{\mathrm{ex2}} = 0.09$. Compared with figure 7a, the bandwidth enhancement is more prominent, which indicates that the damping rate of the laser is more reduced with the increase of OFB from mirror #1 than the increase in OFB from mirror #2.

Pal *et al* [34] observed different frequency responses of semiconductor laser with two filtered OFB, depending on the cavity lengths as well as their relative OFB strengths. Here we are interested in investigating the influence of varying the length of external cavity #2 on the modulation bandwidth $f_{3\,\mathrm{dB}}$ keeping the length of cavity #1 and the corresponding feedback at $L_{\mathrm{ex1}} = 2$ mm and $\eta_1 R_{\mathrm{ex1}} = 0.04$, respectively. Figure 10 plots variation of the bandwidth $f_{3\,\mathrm{dB}}$ with reflectivity $\eta_2 R_{\mathrm{ex2}}$ at two different lengths of cavity #2 of $L_{\mathrm{ex2}} = 2$ mm

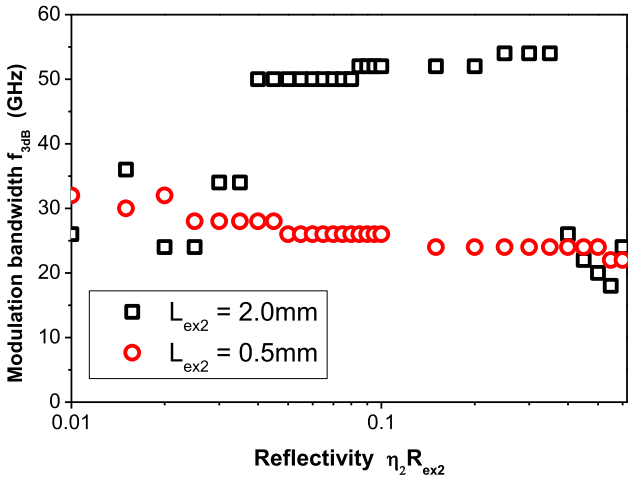

Figure 10. Variation of modulation bandwidth $f_{3\,\mathrm{dB}}$ with reflectivity $\eta_2 R_{\mathrm{ex2}}$ of external mirror #2 when $L_{\mathrm{ex2}} = 2$ mm and 0.5 mm using $\eta_1 R_{\mathrm{ex1}} = 0.04$.

and 0.5 mm. Similar to the case of $L_{\mathrm{ex2}} = 3$ mm in figure 8, the figure shows an increase of $f_{3\,\mathrm{dB}}$ with the increase of $\eta_2 R_{\mathrm{ex2}}$ in the regime of CW operation but with higher maximum value of $f_{3\,\mathrm{dB}} = 54$ GHz when $\eta_2 R_{\mathrm{ex2}} = 0.035$. The CW operation characterising the case of shorter cavity #2 with length $L_{\mathrm{ex2}} = 0.5$ mm corresponds to lower values of the bandwidth $f_{3\,\mathrm{dB}}$. In this case, the largest values of bandwidth are 30 GHz $\leq f_{3\,\mathrm{dB}} \leq$ 38 GHz which correspond to the regime of $\eta_2 R_{\mathrm{ex2}} \leq 0.005$. In the higher levels of $\eta_2 R_{\mathrm{ex2}}$, $f_{3\,\mathrm{dB}}$ ranges between 22 GHz and 28 GHz. That is, higher values of the bandwidth are predicted when cavity #2 is equal to or longer than cavity #1.

5. Conclusions

We introduced theoretical modelling on improvement of the modulation performance and enhancement of the bandwidth of semiconductor lasers subject to DOFB from two external mirrors close to the front and back facets of the laser cavity. The time-delay rate equation model of the semiconductor lasers was modified to include multiple reflections of laser radiation in the two external cavities. We showed that the IM response can be tailored by varying the reflectivity of the external mirrors when the external cavities are too short to stabilise the laser output. When the non-modulated laser operates under CW, strong OFB results in PPR which works to increase the modulation bandwidth. For the present laser parameters, higher values of the bandwidth are predicted when the external cavity facing the front facet is equal to or shorter than the cavity facing the back facet. Values of $f_{3\,\mathrm{dB}}$ reaching 58 GHz were predicted

using external cavity of lengths $L_{ex1} = 2$ mm. When OFB increases more and the non-modulated laser emits period-1 oscillations, the PPR effect causes the modulated laser to exhibit resonant modulation over a narrow frequency range around the PPR frequency which reaches 45 GHz.

Acknowledgements

This project was funded by the Deanship of Scientific Research (DSR) at King Abdulaziz University, Jeddah, under Grant No. (G: 56-130-1441). The authors, therefore, acknowledge with thanks DSR for technical and financial support.

References

[1] X S Qiu, Z M Tuo and Z Yan, *Millimeter wave technology in wireless PAN, LAN and MAN* (Taylor & Francis Group, Boca Raton, 2008)
[2] C Cole, Technol. Digest Optoeletron. Comm. Conf. 108 (2010)
[3] M Sharif, J K Perin and J M Kahn, *J. Lightwave Technol.* **33**(**20**), 4268 (2015)
[4] S Imai *et al*, *Proc. SPIE* **7952**, 795204 (2011)
[5] G P Agrawal and N K Dutta, *Semiconductor lasers* (Van Nostrand Reinhold, New York, 1993)
[6] L A Coldren, S W Corzine and M L Mashanovitch, *Diode lasers and photonic integrated circuits* (John Wiley & Sons, Inc., 1995)
[7] J Wang, M K Haldar, L Li and F V C Mendis, *IEEE Photon. Technol. Lett.* **8**(**1**), 34 (1996)
[8] H Ishihara, Y Saito, W Kobayashi and H Yasaka, *IEICE Trans. Electron.* **E95-C**(**9**), 1549 (2012)
[9] S Mieda, S Shiratori, N Yokota, W Kobayashi and H Yasaka, *Appl. Phys. Express* **8**, 082701 (2015)
[10] H Dalir, M Ahmed, A Bakry and F Koyama, *Appl. Phys. Lett.* **105**(**8**), 081113 (2014)
[11] P Bardella, W Chow and I Montrosset, *Photonics* **3**(**1**), 4 (2016)
[12] M Ahmed, A Bakry, R Altuwirqi, M S Alghamdi and F Koyama, *Jpn. J. Appl. Phys.* **53**(**128**), 124103 (2013)
[13] M Ahmed, A Bakry, R Altuwirqi, M S Alghamdi and F Koyama, *J. Electro-opt. Soc. Rap. Publ.* **8**, 13064 (2013)
[14] M Ahmed, A Bakry, M S Alghamdi, H Dalir and F Koyama, *Opt. Express* **23**, 15365 (2015)
[15] M Ahmed, H Dalir and R Chen, *Optical devices with transverse-coupled cavity*, patent US010658815B1, USA Patent and Trademark Office (2020)
[16] M S Alghamdi, H Dalir, A Bakry, R T Chen and M Ahmed, *Jpn. J. Appl. Phys.* **58**(**11**), 112003 (2019)
[17] H Dalir, A Matsutani, M Ahmed, A Bakry and F Koyama, *IEEE Photon. Technol. Lett.* **26**(**3**), 281 (2014)
[18] H Dalir and F Koyama, *Appl. Phys. Express* **7**, 022102 (2014)
[19] A Murakami and J Ohtsubo, *IEEE J. Quantum Electron.* **34**(**10**), 1979 (1998)
[20] B Tromborg, J H Osmundsen and H Olesen, *IEEE J. Quantum Electron.* **20**(**9**), 1023 (1984)
[21] R W Tkach and A R Chraplyvy, *J. Lightwave Technol.* **4**(**11**), 1655 (1986)
[22] M Yamada, *Theory of semiconductor lasers* (Springer, Tokyo, 2014)
[23] G Duan and G Debarge, *Opt. Lett.* **12**(**10**), 800 (1987)
[24] S Abdulrhmann, M Ahmed, T Okamoto and M Yamada, *IEEE J. Sel. Top. Quantum Electron.* **9**(**5**), 1265 (2003)
[25] K Sato, S H Kuwahara and Y Miyamoto, *J. Lightwave Technol.* **23**(**11**), 3790 (2005)
[26] J Ohtsubo, *Semiconductor lasers: Stability, instability and chaos* (Springer-Verlag, Berlin, 2013) 3rd Edn
[27] J S Cohen, R R Dentine and B H Verbeek, *IEEE J. Quantum Electron.* **24**(**10**), 1989 (1988)
[28] A M Levine, G H M van Tartwijk, D Lenstra and T Erneux, *Phys. Rev. A* **52**, R3436 (1995)
[29] J Helms and K Petermann, *IEEE J. Quantum Electron.* **26**(**5**), 833 (1990)
[30] Y H Kao, N M Wang and H M Chen, *IEEE J. Quantum Electron.* **30**(**8**), 1732 (1994)
[31] M Ahmed, M Yamada and S Abdulrhmann, *Int. J. Numer. Model.* **22**(**6**), 434 (2009)
[32] M Ahmed, *Int. J. Num. Model.* **17**(**2**), 147 (2004)
[33] A Bakry, *Sci. World J.* **2014**, 728458 (2014)
[34] V Pal, J Suelzer, A Prasad, G Vemuri and R Ghosh, *IEEE J. Quantum Electron.* **49**(**3**), 340 (2013)